


Bound states of an ultracold atom interacting with a set of stationary impuritiesMarta Sroczyńska and Zbigniew Idziaszek *Faculty of Physics, University of Warsaw, Ulica Pasteura 5, 02-093 Warsaw, Poland*

(Received 20 July 2020; accepted 16 November 2020; published 9 December 2020)

In this paper we analyze the properties of bound states of an atom interacting with a set of static impurities. We begin with the simplest system of a single atom interacting with two static impurities. We consider two types of atom-impurity interaction: (i) a zero-range potential represented by a regularized δ interaction and (ii) a more realistic polarization potential, representing the long-range part of the atom-ion interaction. For the former we obtain analytical results for energies of bound states. For the latter we perform numerical calculations based on the application of the finite-element method. We then discuss the case of a single atom interacting with a one-dimensional (1D) infinite chain of static ions. Such a setup resembles the Kronig-Penney model of a 1D crystalline solid, where the energy spectrum exhibits band-structure behavior. For this system we derive analytical results for the band structure of bound states, assuming a regularized δ interaction, and perform numerical calculations, considering the polarization potential to model an atom-impurity interaction. Both approaches agree quite well when the separation between impurities is much larger than the characteristic range of the interaction potential.

DOI: [10.1103/PhysRevA.102.063312](https://doi.org/10.1103/PhysRevA.102.063312)**I. INTRODUCTION**

Hybrid systems of ultracold atoms and trapped impurities like ions [1–9] or Rydberg atoms [10,11] have been the subject of intense experimental and theoretical studies over the years [12]. They have been proposed for quantum simulations [13–15], quantum computations [16–18], realization of new mesoscopic quantum states [19,20], probing quantum gases [21–24], and fundamental studies of low-energy collisions and molecular states [25–36]. By tuning the geometric arrangement of the impurities, it is possible to simulate various solid-state and molecular systems [37–40]. Several experiments have been focused on studying controlled chemical reactions at ultralow temperatures in such systems [5,41–45].

In this work we are considering two systems. The first system contains two static impurities, while the second is a one-dimensional (1D) linear crystal of static impurities. We consider two different potentials for atom-impurity interactions, representing two distinct physical systems: atomic impurities in the ultracold gas and the hybrid atom-ion system. For the former we assume a regularized δ potential, while for the latter we take a polarization potential representing the long-range part of the atom-ion interaction, which we regularize at small distances imposing a short-range cutoff. The regularized δ potential models only s -wave scattering at ultralow energies and depends only on a single parameter: the s -wave scattering length. Its zero-range character allows for an analytical solution of the corresponding Schrödinger equation for an arbitrary set of δ -like scatterers [40].

The atom-ion interaction, which has a long-range behavior, can be modeled by including only the long-range part given by the polarization potential $-C_4/r^4$ and a short-range boundary condition. The latter can be represented either by a short-range phase introduced in the framework of the

quantum-defect theory [25] or by regularizing the short-range divergence with some regularizing function [46]. In this work we choose the latter option, assuming parametrization of the atom-ion potential by the long-range dispersion coefficient C_4 and a cutoff radius b . For such a potential one can solve the 1D radial Schrödinger equation analytically and express the scattering length in terms of the C_4 and b parameters [47].

This work is structured as follows. The potentials which we are considering are introduced in Sec. II. In Sec. III we solve the Schrödinger equation for an atom interacting with two impurities and analyze the results for different values of the short-range scattering length. We perform our analysis for atomic impurities, where the atom-impurity interaction is modeled with the δ pseudopotential, and for ionic impurities, where we assume an atom-impurity interaction in the form of the polarization potential. In Sec. IV we consider an infinite chain of ionic impurities. First, we solve the Schrödinger equation numerically using the finite-element method and we discuss numerical solutions of the Schrödinger equation for different values of the atom quasimomentum in a 1D periodic system. Then we derive an analytic formula determining the energies of bound states for the regularized δ potential and study the behavior of energy bands versus the scattering length and distance between impurities. We summarize in Sec. V and present some final conclusions.

II. ATOM-IMPURITY INTERACTION**A. Pseudopotential**

Within the ultracold regime, where mainly s -wave scattering takes place for bosonic or distinguishable particles, we can model the atom-impurity interaction by the Fermi

pseudopotential [48,49] given by

$$V(\mathbf{r}) = g\delta(\mathbf{r})\frac{\partial}{\partial r}r, \quad (1)$$

where g depends on the 3D s -wave scattering length a and

$$g = \frac{2\pi\hbar^2}{m}a. \quad (2)$$

Note that only an atom mass m enters the coupling constant, as we assume that impurities are stationary, and the reduced mass $\mu = m$. Such a potential can serve as a good approximation of a physical potential provided the distance between impurities L is large compared to the characteristic range of the interaction R_n of the power-law potential $V(r) = -C_n/r^n$: $L \gg R_n$. In the case of the atom-ion potential $R_4 = \sqrt{2\mu C_4}/\hbar$, while for the van der Waals potential between neutral atoms $R_6 = (2\mu C_6/\hbar^2)^{1/4}$ [50]. To model bound states we have to impose another constraint $a \gg R_n$, which is equivalent to the condition $E_b \ll E_n$, where the characteristic energy is $E_n = \hbar^2/2\mu R_n^2$ [50]. This shows that the pseudopotential can be used to reproduce bound states in the universal limit, with binding energies E_b that are close to the threshold [51,52]. Going beyond the above-mentioned conditions requires inclusion of the energy-dependent scattering length in (2) [53–55].

B. Regularized atom-ion interaction potential

We will also consider a more realistic potential, such as the polarization potential between atoms and ions. The long-range part of the atom-ion potential is given by $V(\mathbf{r}) \xrightarrow{r \rightarrow \infty} -C_4/r^4$. With this potential we can associate the characteristic length and energy scales that are used further in this work: $R^* = \sqrt{2mC_4}/\hbar$ and $E^* = \hbar^2/2m(R^*)^2$ [56]. Here we will use a regularized version of this long-range potential in the form of the Lenz potential [47], which is finite for $r \rightarrow 0$,

$$V(\mathbf{r}) = -\frac{C_4}{(r^2 + b^2)^2}, \quad (3)$$

where b is a parameter that can be related to the scattering length a [47],

$$a(b) = R^* \sqrt{1 + \left(\frac{b}{R^*}\right)^2} \cot \left[\frac{\pi}{2} \sqrt{1 + \left(\frac{R^*}{b}\right)^2} \right]. \quad (4)$$

This dependence is shown in Fig. 1. We observe that, according to the formula (4), one value of the scattering length can be reproduced by many values of b . The scattering length dependence on b exhibits several resonances that are related to crossing the dissociation threshold by the bound states supported by (3). The number of bound states n is related to the cutoff parameter b by the rule $b \in (b_{n-1}, b_n)$, where $b_n = 1/\sqrt{4n^2 - 1}$.

III. SYSTEM WITH TWO IMPURITIES

We investigate the bound states of the system containing of a single atom that interacts with two impurities placed symmetrically along the z axis such that their positions are $\pm \mathbf{d} = (0, 0, \pm d)$ and the distance between them is $2d$. We assume that each impurity interacts only with the atom and

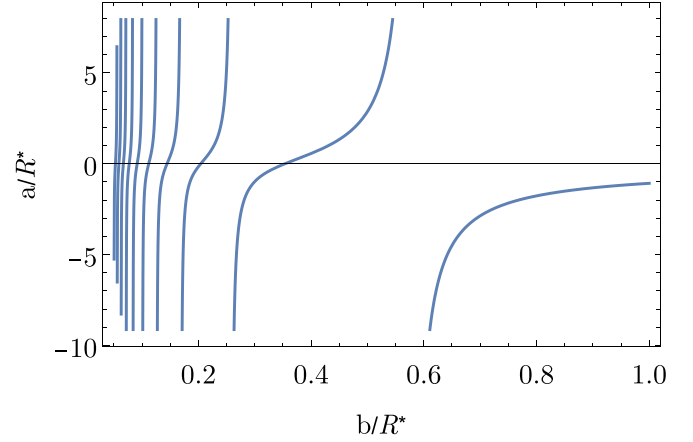


FIG. 1. Scattering length as a function of the regularization parameter given by Eq. (4) for the regularized atom-ion interaction potential (3).

we do not take into account their mutual interactions. We will study the dependence of bound-state energies on the scattering length and on the distance between impurities. The Hamiltonian of such a system is

$$H = -\frac{\hbar^2}{2m}\Delta + V(\mathbf{r} - \mathbf{d}) + V(\mathbf{r} + \mathbf{d}), \quad (5)$$

where V denotes the atom-impurity interaction, which is given by two different atom-impurity potentials introduced in Sec. II.

A. Atom-impurity interaction modeled by the pseudopotential

We solve the Schrödinger equation, using the Green's-function technique. The Green's function for the three-dimensional scattering in free space reads (see, e.g., [57])

$$G(\mathbf{r}, \mathbf{r}') = \mathcal{A} \frac{e^{ik|\mathbf{r}-\mathbf{r}'|}}{|\mathbf{r}-\mathbf{r}'|}, \quad (6)$$

where $\mathcal{A} = -m/2\pi\hbar^2$. Let us define $r_1 = |\mathbf{r} + \mathbf{d}|$ and $r_2 = |\mathbf{r} - \mathbf{d}|$ so that we have

$$G(-\mathbf{d}, \mathbf{r}) = \mathcal{A} \frac{e^{ikr_1}}{r_1} \equiv G(r_1), \quad (7)$$

$$G(\mathbf{d}, \mathbf{r}) = \mathcal{A} \frac{e^{ikr_2}}{r_2} \equiv G(r_2), \quad (8)$$

where for convenience we have also introduced the shortened denotation $G(r_{1(2)})$ for the Green's function. In the case of the Fermi pseudopotential, the Hamiltonian can be solved analytically [40], in principle for an arbitrary arrangement of the impurities. In order to find the energies of the system, we have to solve the set of equations

$$\begin{aligned} k_1 &= g \left\{ \frac{\partial}{\partial r} r [k_1 G(-\mathbf{d}, \mathbf{r}) + k_2 G(\mathbf{d}, \mathbf{r})] \right\}_{\mathbf{r} \rightarrow -\mathbf{d}}, \\ k_2 &= g \left\{ \frac{\partial}{\partial r} r [k_1 G(-\mathbf{d}, \mathbf{r}) + k_2 G(\mathbf{d}, \mathbf{r})] \right\}_{\mathbf{r} \rightarrow \mathbf{d}}, \end{aligned} \quad (9)$$

which can be expressed using the notation with r_1 and r_2 ,

$$k_1 = g \left\{ \frac{\partial}{\partial r_1} r_1 [k_1 G(r_1) + k_2 G(r_2)] \right\}_{r_1 \rightarrow 0}, \quad (10a)$$

$$k_2 = g \left\{ \frac{\partial}{\partial r_2} r_2 [k_1 G(r_1) + k_2 G(r_2)] \right\}_{r_2 \rightarrow 0}. \quad (10b)$$

The regularization operator $\frac{\partial}{\partial r} r$ is necessary as it ensures that the limit $[G(\mathbf{r}, \mathbf{r}')]_{|\mathbf{r}-\mathbf{r}'| \rightarrow 0}$ is finite [58,59]. It can be omitted in the case of the one-dimensional system, when the Green's function is not divergent at short distances. The wave function of the system is given by

$$\Psi(\mathbf{r}) = k_1 G(-\mathbf{d}, \mathbf{r}) + k_2 G(\mathbf{d}, \mathbf{r}). \quad (11)$$

Let us now calculate the derivatives of the Green's function that appear in Eq. (10a) and their values in the limit of $r_1 \rightarrow 0$:

$$\begin{aligned} \left(\frac{\partial}{\partial r_1} r_1 G(r_1) \right)_{r_1 \rightarrow 0} &= \mathcal{A} \left(\frac{\partial}{\partial r_1} r_1 \frac{e^{ikr_1}}{r_1} \right)_{r_1 \rightarrow 0} \\ &= \mathcal{A} \left(\frac{\partial}{\partial r_1} e^{ikr_1} \right)_{r_1 \rightarrow 0} \\ &= \mathcal{A} ik (e^{ikr_1})_{r_1 \rightarrow 0} = \mathcal{A} ik. \end{aligned} \quad (12)$$

Then we have

$$\begin{aligned} \left(\frac{\partial}{\partial r_1} r_1 G(r_2) \right)_{r_1 \rightarrow 0} &= \mathcal{A} \left(\frac{\partial}{\partial r_1} r_1 \frac{e^{ikr_2}}{r_2} \right)_{r_1 \rightarrow 0} \\ &= \mathcal{A} \left(\frac{e^{ikr_2}}{r_2} + r_1 \frac{\partial}{\partial r_1} \frac{e^{ikr_2}}{r_2} \right)_{r_1 \rightarrow 0} \\ &= \mathcal{A} \frac{e^{ik2d}}{2d}. \end{aligned} \quad (13)$$

Derivatives of the Green's function and their limits for $r_2 \rightarrow 0$, appearing in Eq. (10b) can be calculated in an analogous way. Now we insert the obtained results into the system of equations (10):

$$\begin{aligned} k_1 &= g \mathcal{A} \left(k_1 ik + k_2 \frac{e^{ik2d}}{2d} \right), \\ k_2 &= g \mathcal{A} \left(k_1 \frac{e^{ik2d}}{2d} + k_2 ik \right). \end{aligned} \quad (14)$$

The expression (14) can be rewritten in matrix form as

$$\begin{pmatrix} g \mathcal{A} ik - 1 & g \mathcal{A} \frac{e^{ik2d}}{2d} \\ g \mathcal{A} \frac{e^{ik2d}}{2d} & g \mathcal{A} ik - 1 \end{pmatrix} \begin{pmatrix} k_1 \\ k_2 \end{pmatrix} = 0. \quad (15)$$

This system of equations has solutions provided that the determinant of the matrix is equal to zero. From this condition we get two independent solutions

$$g \mathcal{A} \left(ik \pm \frac{e^{ik2d}}{2d} \right) - 1 = 0. \quad (16)$$

Since we are looking for bound states, the wave number $k = ik$ where κ is real, the energy $E = -\frac{\hbar^2 \kappa^2}{2m}$, and $\kappa = \sqrt{-2mE/\hbar^2}$. Taking into account that $g \mathcal{A} = -a$, we can

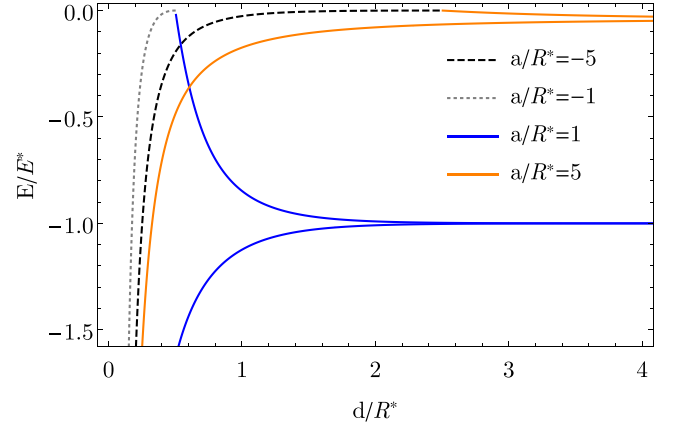


FIG. 2. Energy spectrum resulting from (17), the energy levels of a system consisting of an atom interacting with two impurities by the δ pseudopotential with different scattering lengths: $a/R = -5$ (black dashed line), $a/R^* = -1$ (gray dotted line), $a/R^* = 1$ (blue solid line), and $a/R^* = 5$ (orange solid line).

rewrite the expression (16) as

$$-\kappa \pm \frac{e^{-\kappa 2d}}{2d} = \frac{1}{a}. \quad (17)$$

The energy levels can now be found numerically for a given value of the scattering length and d . At the threshold $E = \kappa = 0$ Eq. (17) yields

$$\pm \frac{1}{2d} = \frac{1}{a}, \quad E = 0. \quad (18)$$

From this we see that, at the distance $d = |a|/2$, the new bound state either appears or disappears at the threshold, depending on the sign of the scattering length.

Let us now consider two limiting cases. In the limit $d \rightarrow 0$, from Eq. (17) we obtain

$$\kappa \xrightarrow{d \rightarrow 0} \pm \frac{1}{2d}, \quad (19)$$

which diverges as d goes to zero. This singular behavior results from the Green's function in the off-diagonal terms, which are not regularized by the $\frac{\partial}{\partial r} r$ operator and as a consequence yields divergence at $d \rightarrow 0$. It is possible to reformulate a regularization operator in the way that it correctly reproduces the limit of two δ functions [32]. We note, however, that the limit $d \rightarrow 0$ corresponds physically to combining two impurities in a single molecular complex, which in principle would have a scattering length different from the sum of the two scattering lengths of the separate objects. In the case where the separation of the impurities is very large ($d \rightarrow \infty$), the term $e^{-2d\kappa}/2d$ goes to zero and we get $a\kappa = 1$, which implies the existence of the bound state for positive values of the scattering length

$$E \xrightarrow{d \rightarrow \infty} -\frac{\hbar^2}{2ma^2} \quad (20)$$

and no bound states in the case of $a < 0$.

Figure 2 compares bound-state energies evaluated from Eq. (17) for different values of the scattering length. For positive scattering lengths, at large distances the bound state

energies are degenerate and tend to the energy of a single bound state (20). In contrast, for negative scattering lengths, there are no bound states at large distances, as the separate δ potential does not support any bound states for $a < 0$. Nevertheless, at distances $d < |a|/2$, the two impurities pose a single bound state, crossing the threshold at $d = |a|/2$. At exactly the same distance, for positive scattering lengths, one of the bound states disappears at the threshold and for $d < |a|/2$ the two impurities support again only a single bound state. We note that for $d > |a|/2$, Eq. (17) is not valid for negative scattering lengths.

B. Atom-impurity interaction modeled by the regularized atom-ion potential

In this case, we cannot solve the Hamiltonian analytically and we have to rely on numerics. We begin by looking for eigenstates for a single ion, using two different numerical methods: the Numerov algorithm and the finite-element method. This comparison helps to adjust the parameters of the grid in the finite-element method, which we later use to solve the two-ion case.

1. Single-ion case

The interaction potential for a single ion is spherically symmetric. Therefore, the wave function can be decomposed as $\psi(\mathbf{r}) = \mathcal{R}(r)Y_{lm}(\theta, \phi)$, where $\mathcal{R}(r)$ is the radial part and $Y_{lm}(\theta, \phi)$ is the spherical harmonic, with quantum numbers l and m representing the angular momentum and its projection on the z axis, respectively. In order to find the bound states, we only need to solve the radial part of the Schrödinger equation. It is convenient to look for $\mathcal{R}(r)/r$, which simplifies the Laplacian operator but does not affect the energies. The Hamiltonian to solve reads

$$H = -\frac{\hbar^2}{2m} \frac{d^2}{dr^2} + \frac{\hbar^2}{2m} \frac{l(l+1)}{r^2} - \frac{C_4}{(r^2 + b^2)^2}. \quad (21)$$

a. Numerov method. With the Numerov algorithm we solve the Schrödinger on a grid of equally spaced points between $r = r_{\min}$ and $r = r_{\max}$, assuming that the wave function vanishes at the boundaries. In principle, r_{\max} should be much larger than R^* and a . For our computations we take $r_{\min} = 0$ and $r_{\max} = 20R^*$.

b. Finite-element method. In this case, we are solving the Schrödinger equation

$$-\frac{\hbar^2}{2m} \Delta \psi - \frac{C_4}{(\rho^2 + z^2 + b^2)^2} \psi = E \psi. \quad (22)$$

It is convenient to rewrite this equation in the cylindrical coordinates

$$-\frac{\hbar^2}{2m} \left(\frac{\partial^2}{\partial z^2} + \frac{\partial^2}{\partial \rho^2} + \frac{1}{\rho} \frac{\partial}{\partial \rho} \right) \psi + \frac{C_4}{(\rho^2 + z^2 + b^2)^2} \psi = E \psi, \quad (23)$$

where additionally we assumed an $m = 0$ symmetry of the solutions.

In order to find the energy levels of the system, we solve Eq. (23) numerically using the finite-element method implemented in the *Mathematica* software [60]. We perform

calculations for a single ion placed at the origin of the coordinate system, in a rectangular box, with $-z_{\max} \leq z \leq z_{\max}$ and $0 \leq \rho \leq \rho_{\max}$. The values of ρ_{\max} and z_{\max} should be relatively large compared to the scattering length in order to preclude the bound-state wave functions being affected by the boundary conditions. For our computations we take $z_{\max} = 8R^*$ and $\rho_{\max} = 8R^*$. We assume the Dirichlet boundary condition $\psi = 0$ along all the boundaries except $\rho = 0$, where we set the von Neumann boundary condition $\frac{\partial}{\partial \rho} \psi(\rho = 0, z) = 0$. The regularization parameter b is set such that one bound state is supported for a given scattering length. It is worth noting that close to the ion, the potential is getting relatively deep and the corresponding wave function becomes quickly oscillating in that region. To address this issue we use a variable grid size related to the local de Broglie wavelength $\lambda(\mathbf{r}, E) = 2\pi/\sqrt{2m|E - V_{\text{ai}}(\rho, z)|/\hbar^2}$, by assuming that the area of a single cell in the grid fulfills $\Delta \leq \lambda(\mathbf{r}, E)^2/N^2$. We test several values of the N parameter, observing that numerical calculations start converging for $N \gtrsim 20$ in the case of the atom-ion potential supporting one bound state and $N \gtrsim 30$ for deeper potentials supporting two bound states. An example grid is shown in Fig. 3.

Figure 4 shows the energies of bound states obtained using both methods for $l = 0, 1, 2$. We note that both numerical approaches give almost identical results, which substantiates the numerical convergence of both methods.

2. Two-ion case

We now turn to the system of two ions. We solve the Schrödinger equation with the Hamiltonian (5), using the finite-element method with the same boundary conditions as in the single-ion case. The value of the cutoff parameter b is chosen such that the potential is relatively shallow and only one or two bound states are supported. In contrast to the pseudopotential model, now we obtain finite results for both small and large separations between the impurities.

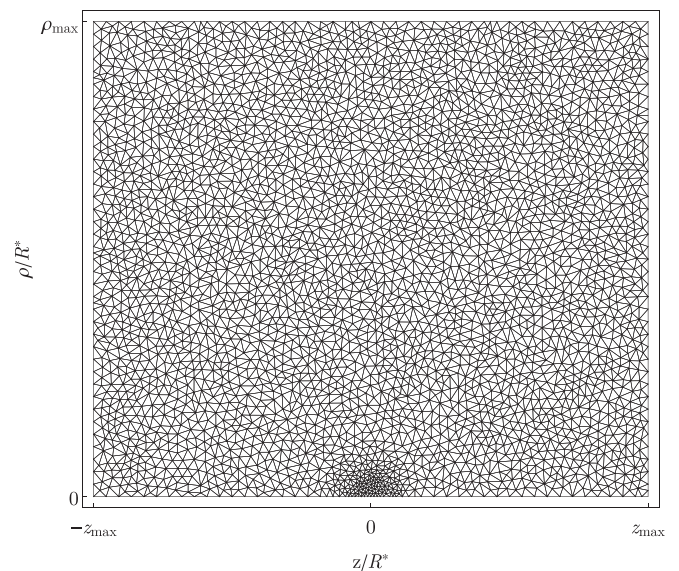


FIG. 3. Example grid used for the finite-element method. The grid size is determined by the local de Broglie wavelength and it becomes very dense in the vicinity of the ion at $z = 0$ and $\rho = 0$.

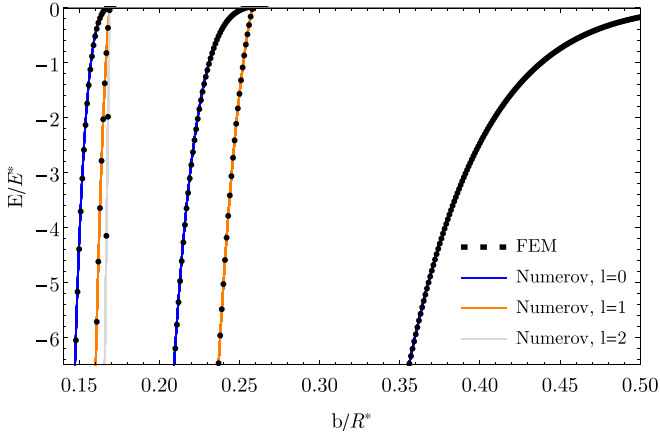


FIG. 4. Energies of bound states in a regularized atom-ion potential for different values of b computed using the Numerov algorithm (blue, orange, and light gray lines correspond to the angular momenta $l = 0, 1$, and 2 , respectively) and the finite-element algorithm (black points).

In Fig. 5 we plot the energies of bound states for different values of the scattering length a and for the cutoff parameter b as a function of distance d between impurities. In

addition, we include the predictions of the pseudopotential model (17). For $a > 0$ and $d \rightarrow \infty$, the impurities do not encounter each other and the bound-states energies tend asymptotically to the values for a single impurity (dashed line), calculated from (21) using the Numerov method. Bound states for the polarization potential behave basically in a similar way as for the pseudopotential. At some finite distance, which is now different for positive and negative scattering lengths, bound states for the polarization potential cross the threshold, and below that characteristic distance, the system supports only a single shallow bound state. We note that for large scattering lengths $a = \pm 5R^*$, the crossing point is similar for potentials supporting one and two bound states. In contrast, for $a = \pm R^*$, the crossing point is quite different between these potentials and it also deviates from the pseudopotential prediction $d = |a|/2$. This is probably due to the finite-size effects when $a \sim R^*$. We suppose that replacement of the scattering length by the energy-dependent one [53–55] would possibly improve the agreement, at least for the pseudopotential model.

Similar discrepancies can be observed at large distances for $a = R^*$, where all three calculations predict various asymptotic values for the bound state of a separated impurity. The

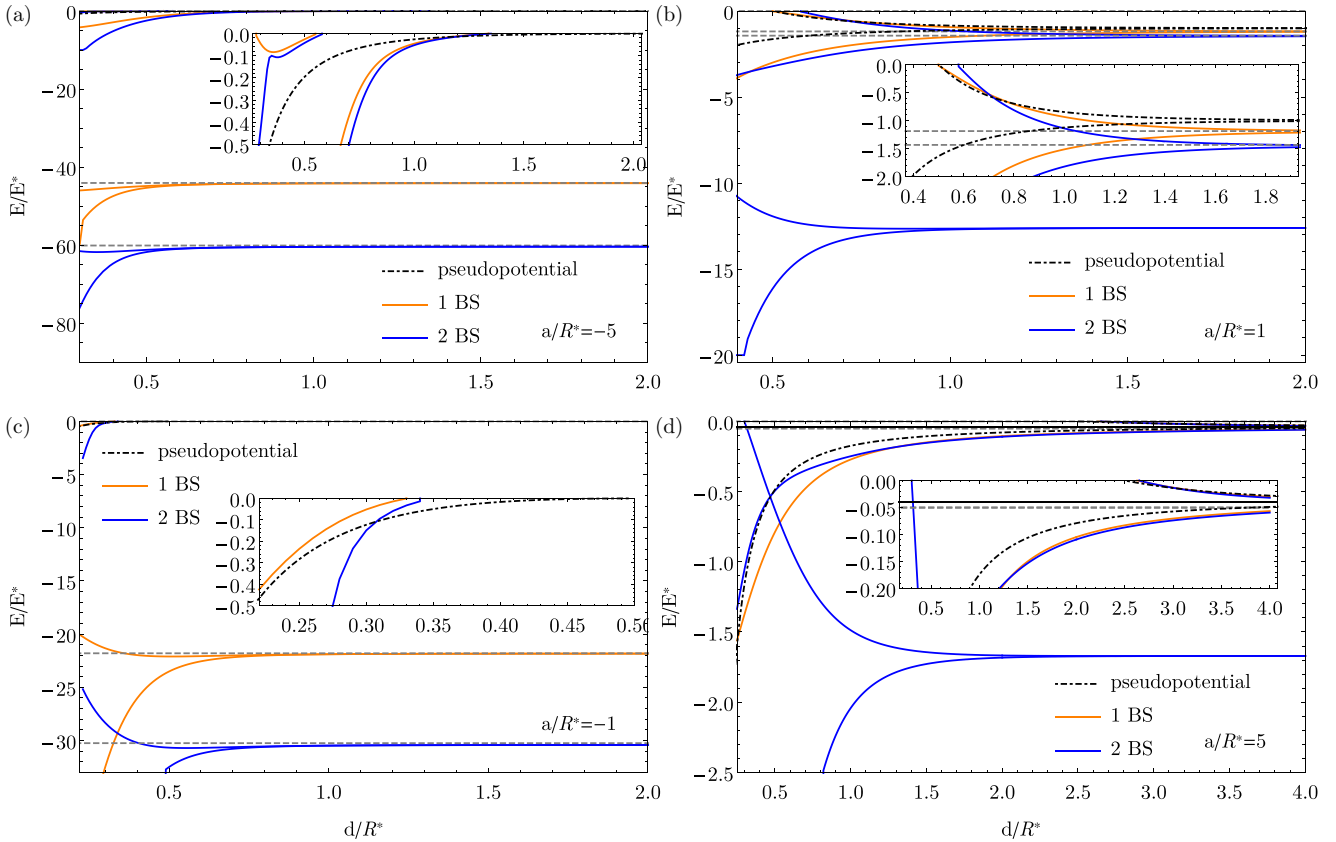


FIG. 5. Energy spectrum as a function of d (half of the distance between the impurities) for different values of the scattering length a and corresponding regularization parameter b supporting one bound state (orange lines) or two bound states (blue lines): (a) $a/R^* = -5$ and $b/R^* = 0.26748$ (orange) or $b/R^* = 0.17281$ (blue), (b) $a/R^* = 1$ and $b/R^* = 0.43089$ (orange) or $b/R^* = 0.22749$ (blue), (c) $a/R^* = -1$ and $b/R^* = 0.29942$ (orange) or $b/R^* = 0.18509$ (blue), and (d) $a/R^* = 5$ and $b/R^* = 0.52804$ (orange) or $b/R^* = 0.24959$ (blue). The black dot-dashed line shows the energy spectrum calculated with the pseudopotential. The gray dashed line corresponds to the bound state in the large- d limit, calculated for a single impurity.

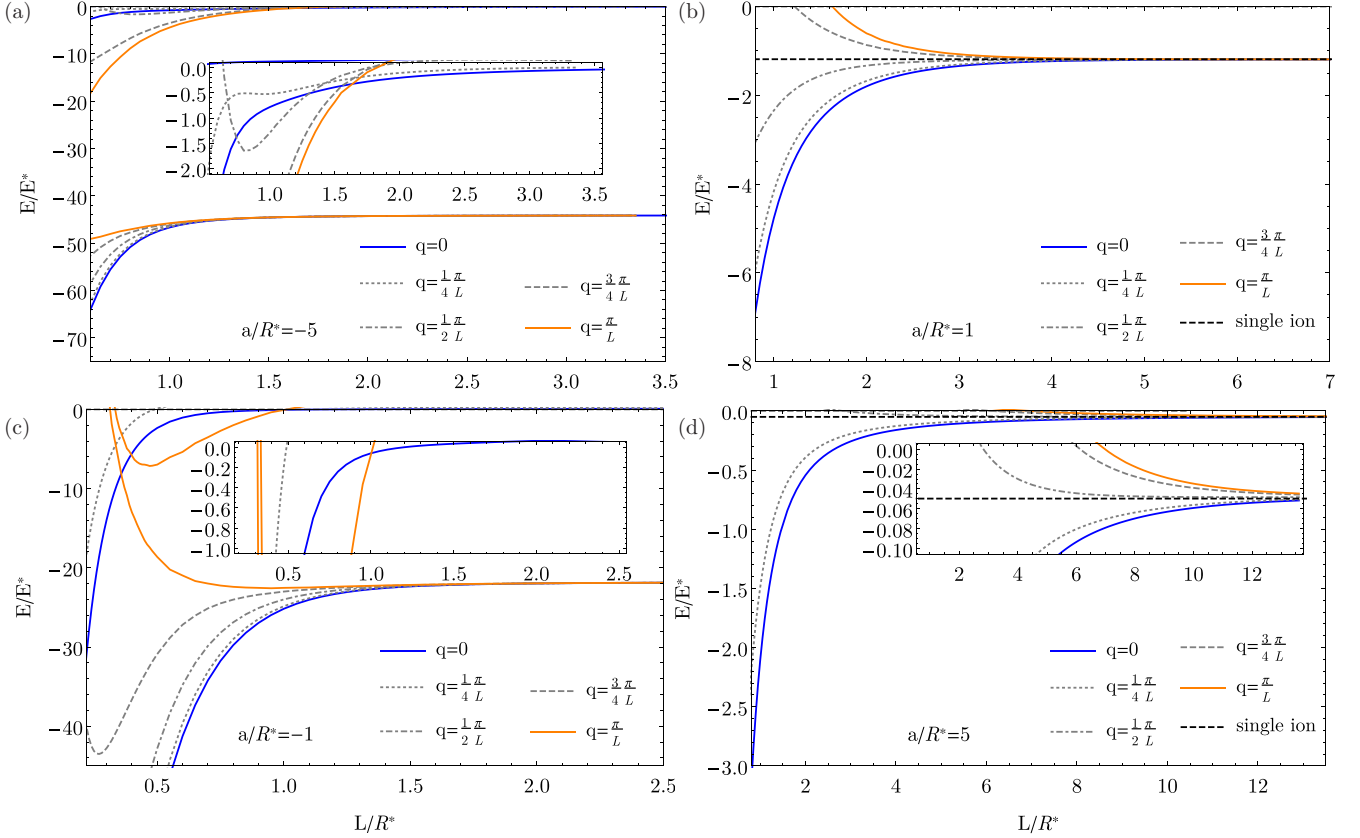


FIG. 6. Energy levels of an atom interacting with a periodic system of impurities as a function of the period for different values of scattering length and corresponding regularization parameter: (a) $a/R^* = -5$ and $b/R^* = 0.26748$, (b) $a/R^* = 1$ and $b/R^* = 0.43089$, (c) $a/R^* = -1$ and $b/R^* = 0.29942$, and (d) $a/R^* = 5$ and $b/R^* = 0.52804$. The atom-impurity interaction is modeled by the regularized atom-ion potential. The insets show close-ups of the spectrum close to $E = 0$. Blue lines denote the solutions of (26) with $q = 0$ and orange lines are the results of (26) with $q = \pi/L$. Gray dotted, dot-dashed, and dashed lines correspond to $q = \pi/4L$, $\pi/2L$, and $3\pi/4L$, respectively.

agreement is much better for higher value of the scattering length $a = 5R^*$. When the distance between impurities is getting close to zero, the bound states calculated for various models show different behavior. In such a case our models break down and we do not show this limit in the plot. This happens for the pseudopotential model because d is not larger than R^* and the conditions for the applicability of the pseudopotential approximation are no longer fulfilled. For the regularized atom-ion potential, at distances d comparable to the cutoff parameter b , the potentials start to overlap significantly, and in this case the results depend on b , determining the number of bound states in the regularized potential. In all the panels we observe the deeply lying bound states supported by the regularized atom-ion potential. Their energies, however, substantially depend on the number of bound states supported by the potential, and even at the same value of the scattering length they differ. Those deeper lying bound states are not the target of our analysis.

IV. PERIODIC SYSTEM

Here we consider an atom interacting with an infinite chain of equally spaced static ions. The interaction V_{ai} is given by the regularized atom-ion potential (Sec. II B). Similarly to the two-ion case, we neglect the interaction between the ions. The

Hamiltonian reads

$$H = -\frac{\hbar^2}{2m}\Delta - \sum_{n=-\infty}^{\infty} V(\mathbf{r} - \mathbf{d}_n), \quad (24)$$

where $\mathbf{d}_n = (0, 0, nL)$ is the position of n th ion and L is the distance between the neighboring ions (period). The ions are placed along the z axis.

Exploiting the fact that the system is axially symmetric and periodic along the z axis and taking into account the Bloch theorem, we can write the wave function in cylindrical coordinates ρ and z in the form

$$\psi(\mathbf{r}) = e^{iqz} u_q(\rho, z) e^{im\phi}, \quad (25)$$

where q is the quasimomentum. In the following we consider only the eigenstates with the symmetry $m = 0$. Substituting (25) into the Schrödinger equation with the Hamiltonian (24) leads to the following equation for u_q :

$$-\frac{\hbar^2}{2m} \left(\frac{\partial^2}{\partial z^2} + \frac{\partial^2}{\partial \rho^2} - q^2 + 2iq \frac{\partial}{\partial z} + \frac{1}{\rho} \frac{\partial}{\partial \rho} \right) u_q(\rho, z) - \sum_{n=-\infty}^{\infty} V(\mathbf{r} - \mathbf{d}_n) u_q(\rho, z) = E u_q(\rho, z). \quad (26)$$

A. Atom-impurity interaction modeled by the regularized atom-ion potential

In order to find the energy levels of the system, we solve Eq. (26) numerically using the finite-element method, in a manner similar to that described for the two-ion system. We perform calculations for an ion placed in the position $\mathbf{d} = (0, 0, L/2)$ in the rectangular box with $z \in [0, L]$ and $\rho \in [0, \rho_{\max}]$. The value of ρ_{\max} should be large compared to the scattering length in order to not affect the bound-state wave functions, and we take $\rho_{\max} = 6R^*$ for $a/R^* = \pm 1$ and $\rho_{\max} = 10R^*$ for $a/R^* = \pm 5$. For $\rho = \rho_{\max}$ we assume the Dirichlet boundary condition $u_q(\rho_{\max}, z) = 0$, while for $\rho = 0$ we assume the von Neumann boundary condition $\frac{\partial}{\partial \rho} u(\rho = 0, z) = 0$. The function u_q should be periodic in the z direction, so for $z = 0$ and $z = L$ we set periodic boundary conditions. The regularization parameter b is set such that one bound state is supported for a given scattering length. In Fig. 6 we show how the energy levels change with the distance between the neighboring ions for different values of the scattering length and some selected values of the quasimomentum q . We start by discussing the case of $a > 0$, i.e., Figs. 6(b) and 6(d). At large distances between the neighboring impurities, the energy levels for different q converge to the same limit and the band becomes very narrow. This asymptotic value is given by the energy of the bound state associated with a single impurity. As the distance L between the impurities decreases, the energy band becomes wider and some bound states cross the threshold, starting with the quasimomentum $q = \pi/L$.

For $a < 0$ [Figs. 6(a) and 6(c)], the energy bands have an even more complex structure. At large separations between the impurities, for each quasimomentum there is a single bound state, which at $L \rightarrow \infty$ tends to the energy of the bound state localized on a single ion. This represents a deeply lying bound state of the atom-ion potential, and close to the threshold there are no bound states in this regime, similarly to the two-ion system. As the ion separation decreases, some bound states cross the threshold entering from the continuum, and later different energy bands start to overlap. This process actually begins for a bound state with $q = 0$ and continues to $q = \pi/L$, as can be seen in Fig. 6(a) ($a = -5R^*$). For $a = -R^*$, probably due to the finite-range effects, this behavior is quite different. We can observe that between bound states with $q = 0$ and $q = \pi/L$, there are no other states crossing the threshold.

Figure 7 shows some exemplary wave functions of the bound states. The presented wave functions are, to a large extent, spherically symmetric. The wave function has the form of a linear combination of bound-state wave functions centered at individual impurities. In this sense our ansatz resembles the linear combination of atomic orbitals method of quantum chemistry. However, in our case it leads to an exact solution, not requiring variational calculations.

B. Atom-impurity interaction modeled by the pseudopotential

We now turn to the analytical calculation of the energy spectrum for an atom interacting with a chain of impurities, where the interaction is modeled by the pseudopotential (1). We solve the problem using the Green's-function

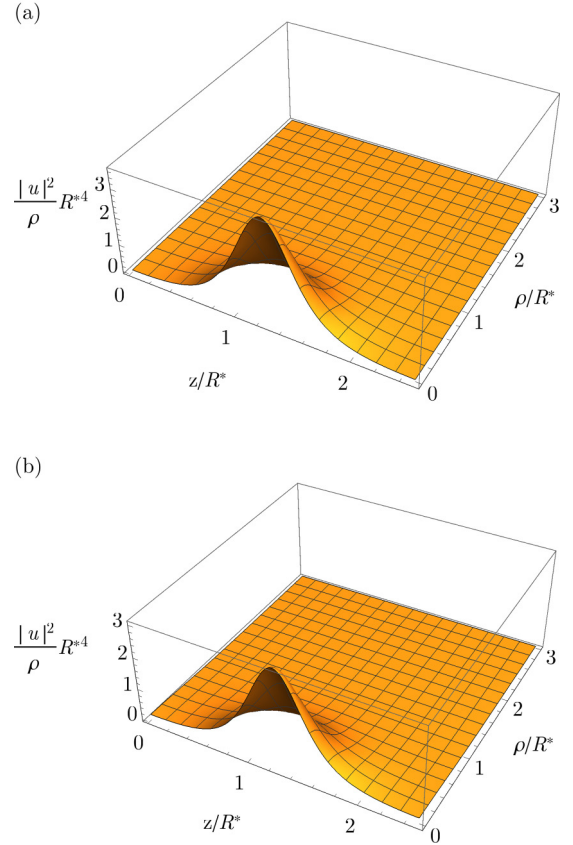


FIG. 7. Wave functions for (a) $a/R^* = 1$, $L/R^* = 2.5$, and $q = \pi/L$ ($E/E^* = -0.93$) and (b) $a/R^* = 1$, $L/R^* = 2.5$, and $q = 0$ ($E/E^* = -1.49$). An impurity is placed at $(z, \rho) = (L/2, 0)$.

technique, starting from the Lippmann-Schwinger equation (see, e.g., [57]). This yields

$$\psi(\mathbf{r}) = \int d^3r' G(\mathbf{r}, \mathbf{r}') \sum_{n=-\infty}^{\infty} V(\mathbf{r}' - \mathbf{d}_n) \psi(\mathbf{r}'), \quad (27)$$

where we drop inhomogeneous term, which is not important for the bound states. In order to calculate the integral, we insert the atom-impurity interaction potential (1) into (27), which gives

$$\psi(\mathbf{r}) = g \sum_{n=-\infty}^{\infty} G(\mathbf{r}, \mathbf{d}_n) \gamma_n, \quad (28)$$

where

$$\gamma_n = \left(\frac{\partial}{\partial r_n} r_n \psi(\mathbf{r}) \right)_{\mathbf{r} \rightarrow \mathbf{d}_n} \quad (29)$$

and $\mathbf{r}_n = \mathbf{r} - \mathbf{d}_n$. Since the potential is periodic along the z axis, using the Bloch theorem, we can rewrite the wave function ψ as

$$\psi(\mathbf{r}) = e^{iqz} \phi(\mathbf{r}), \quad (30)$$

where ϕ is periodic and satisfies $\phi(\mathbf{r}) = \phi(\mathbf{r} - \mathbf{d}_n)$. Substituting (30) into the expression (29) for γ_n , we get

$$\gamma_n = \left(\frac{\partial}{\partial r_n} r_n e^{iqz} \phi(\mathbf{r}) \right)_{\mathbf{r} \rightarrow \mathbf{d}_n} = C e^{iqnL}, \quad (31)$$

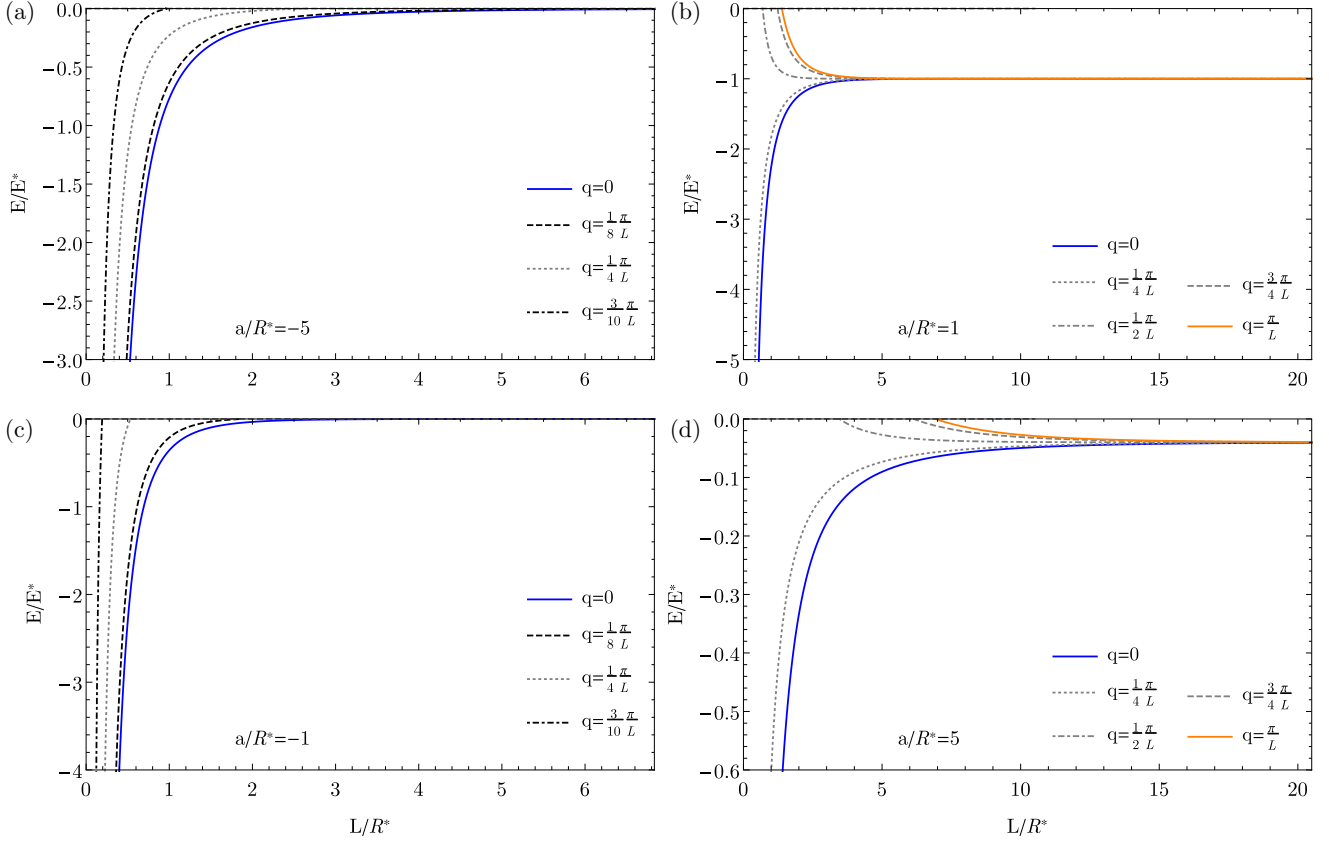


FIG. 8. Energy levels of an atom interacting with a periodic system of impurities as a function of the period for different values of scattering length: (a) $a/R^* = -5$, (b) $a/R^* = 1$, (c) $a/R^* = -1$, and (d) $a/R^* = 5$. The atom-impurity interaction is modeled by the regularized pseudopotential. Blue lines denote the solutions of (26) with $q = 0$ and orange lines are the results of (41) with $q = \pi/L$. Gray dotted, dot-dashed, and dashed lines correspond to $q = \pi/4L$, $\pi/2L$, and $3\pi/4L$, respectively. Black dashed and dot-dashed lines correspond to $q = \pi/8L$ and $3\pi/10L$, respectively.

where

$$\mathcal{C} = \left(\frac{\partial}{\partial r_n} r_n \phi(\mathbf{r}_n) \right)_{\mathbf{r}_n \rightarrow 0}. \quad (32)$$

The specific value of \mathcal{C} is not important, as it drops out in further calculations. Since the regularization operator removes $1/r$ singularity from the short-range behavior of the wave function, we can assume that \mathcal{C} is finite. Now we insert the wave function ψ defined in (28) into the definition of γ_n (29), which leads to

$$\begin{aligned} \gamma_n &= g \left(\frac{\partial}{\partial r_n} r_n \sum_{n'=-\infty}^{\infty} G(\mathbf{r}, \mathbf{d}_{n'}) \gamma_{n'} \right)_{\mathbf{r}_n \rightarrow 0} \\ &= g \left(\gamma_n \beta(E) + \sum_{n' \neq n} G(\mathbf{d}_n, \mathbf{d}_{n'}) \gamma_{n'} \right), \end{aligned} \quad (33)$$

where we have introduced

$$\beta(E) = \left(\frac{\partial}{\partial r} r G(\mathbf{r} + \mathbf{d}_n, \mathbf{d}_n) \right)_{\mathbf{r} \rightarrow 0}. \quad (34)$$

We have obtained two expressions for γ_n , (31) and (33), which yield the equation

$$\mathcal{C} e^{iqnL} = g \mathcal{C} \left(\beta(E) e^{iqnL} + \sum_{n' \neq n} e^{iqn'L} G(\mathbf{d}_n, \mathbf{d}_{n'}) \right). \quad (35)$$

We can now simplify (35), dividing both sides by \mathcal{C} and multiplying by e^{-iqnL} , which gives

$$1 = g \left(\beta(E) + \sum_{n' \neq n} e^{iq(n'-n)L} G(\mathbf{d}_n, \mathbf{d}_{n'}) \right). \quad (36)$$

The value of the Green's function in (36) is

$$G(\mathbf{d}_n, \mathbf{d}_{n'}) = \mathcal{A} \frac{e^{ik|n-n'|L}}{L|n-n'|}, \quad (37)$$

while $\beta(E)$ is

$$\beta(E) = \left(\frac{\partial}{\partial r} r \mathcal{A} \frac{e^{ikr}}{r} \right)_{r \rightarrow 0} = \mathcal{A} ik = -\mathcal{A} \kappa, \quad (38)$$

where $\kappa = ik$ is real for eigenstates with negative energies. After inserting (38) and (37) into the right-hand side of (36)

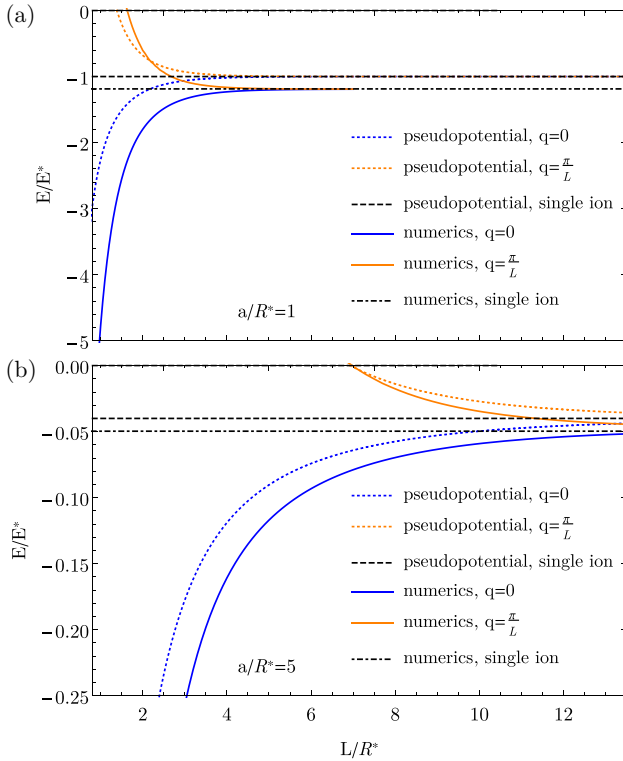


FIG. 9. Comparison of the energies of bound states obtained numerically (solid lines) and analytically (dotted lines) for (a) $a/R^* = 1$ and (b) $a/R^* = 5$. Blue and orange lines correspond to $q = 0$ and $q = \pi/L$, respectively. The black dashed and dot-dashed lines depict bound-state energies for a single ion, calculated from the radial equation using the Numerov and pseudopotential methods, respectively.

we obtain

$$g\left(\beta(E) + \sum_{n' \neq n} e^{iq(n'-n)L} G(\mathbf{d}_n, \mathbf{d}_{n'})\right) = \frac{a}{L} \{\kappa L + \ln[(1 - e^{-\kappa L + iqL})(1 - e^{-\kappa L - iqL})]\}, \quad (39)$$

where we have used the series expansion of the logarithm function in order to make the summation

$$\sum_{n=1}^{\infty} \frac{z^n}{n} = -\ln(1 - z). \quad (40)$$

This holds, provided $|z| < 1$ [in our case $|z| = |\exp(-\kappa L)|$, so the condition $\kappa > 0$ has to be satisfied]. Finally, we need to solve

$$\frac{L}{a} = \ln[\cosh(\kappa L) - \cos(qL)] + \ln 2 \quad (41)$$

for κ , which results in the solution

$$\kappa = \frac{1}{L} \operatorname{arcosh}\left(\cos(qL) + \frac{1}{2}e^{L/a}\right). \quad (42)$$

The solutions of this equation are shown in Fig. 8, presenting energy bands of bound states for different values of the scattering length and the quasimomentum, as a function of the impurity spacings. Basically, we observe behavior very similar to that in the case of the atom-ion potential, except

that the δ pseudopotential does not support bound states for $a < 0$. Due to the same argument, there are no deep bound states in the spectrum, as observed for atom-ion potential. For negative scattering lengths, the plots present only the curves for relatively small q , because for larger q , Eq. (41) predicts imaginary κ , when $\cos(qL) + \frac{1}{2}e^{L/a} < 1$.

In Fig. 9 we plot bound-state energies for positive values of the scattering length and some selected quasimomenta, comparing two types of atom-impurity interactions considered in the paper. We observe that in the case of the ionic chain, the pseudopotential method works definitely worse than for the two-ion system. Similarly to the case of two impurities, the asymptotic value at $L \rightarrow \infty$ obtained from numerics for the atom-ion potential is slightly lower than for the pseudopotential, which is due to the finite-range effects.

V. SUMMARY

In this work we have considered bound states of an atom interacting with different setups of static impurities. First, we calculated energies of bound states for two δ pseudopotentials and showed that they can even exist for negative values of the scattering length, which is not possible for a single atomic impurity. Such bound states, however, exist only when the distance between impurities is smaller than some characteristic value of the order of the scattering length. Similar behavior is observed when we consider a long-range polarization potential. On the other hand, for positive values of the scattering length and at large distances between impurities, there are two solutions for bound-state energies. In the asymptotic limit they tend to the energy of a single atom-impurity molecular state. At smaller distances, the degeneracy is lifted and at some characteristic distance between impurities, one of the bound disappears at the threshold. Calculations performed for the atom-ion polarization potential show that it exhibits a similar behavior.

For an infinite chain of ionic impurities, we observe behavior roughly analogous to that for two ions. In this case bound states aggregate into bands. For positive values of the scattering length, the energy bands at large separations between ions correlate with energies of a separate atom-ion bound state. For negative values of the scattering length, the shallowest energy band disappears at large ion separations. Finally, we extended our analytical calculations performed for two impurities to the case of a 1D infinite chain of δ -like impurities. We derived a relatively simple analytical equation determining the energy levels of bound states for this system. In principle, our results are valid for nonmoving impurities, but they can be a good approximation also when the impurities are much heavier than atoms. For such conditions, the motion of heavy impurities can be treated in the framework of the Born-Oppenheimer approximation, and solving the Schrödinger equation for the motion of light atoms in the potential of the stationary impurities is the first necessary step. Our treatment can be applied also for a system of ionic impurities, where the ions typically perform small oscillations around equilibrium positions, leading to the occurrence of phonons [13].

In future investigations the energy-dependent scattering length should be included in the δ pseudopotential [53,54], which would allow the finite-range effect of the potential to

be accounted for. Assuming the energy dependence appropriate for the polarization potential, in principle one should be able to better reproduce the numerical calculations performed with the finite-element method for the ionic chain and explain the behavior of the energy bands for smaller values of a . This would require, however, generalization of the energy-dependent scattering length for the polarization po-

tential to the negative energies, which so far has been only realized for van der Waals interactions [55].

ACKNOWLEDGMENT

This work was supported by the National Science Center Grant No. 2014/14/M/ST2/00015.

-
- [1] W. W. Smith, O. P. Makarov, and J. Lin, *J. Mod. Opt.* **52**, 2253 (2005).
- [2] A. T. Grier, M. Cetina, F. Oručević, and V. Vuletić, *Phys. Rev. Lett.* **102**, 223201 (2009).
- [3] C. Zipkes, S. Palzer, C. Sias, and M. Köhl, *Nature (London)* **464**, 388 (2010).
- [4] S. Schmid, A. Härter, and J. H. Denschlag, *Phys. Rev. Lett.* **105**, 133202 (2010).
- [5] F. H. J. Hall, M. Aymar, N. Bouloufa-Maafa, O. Dulieu, and S. Willitsch, *Phys. Rev. Lett.* **107**, 243202 (2011).
- [6] S. T. Sullivan, W. G. Rellergert, S. Kotochigova, and E. R. Hudson, *Phys. Rev. Lett.* **109**, 223002 (2012).
- [7] K. Ravi, S. Lee, A. Sharma, G. Werth, and S. A. Rangwala, *Nat. Commun.* **3**, 1126 (2012).
- [8] K. S. Kleinbach, F. Engel, T. Dieterle, R. Löw, T. Pfau, and F. Meinert, *Phys. Rev. Lett.* **120**, 193401 (2018).
- [9] T. Feldker, H. Fürst, H. Hirzler, N. V. Ewald, M. Mazzanti, D. Wiater, M. Tomza, and R. Gerritsma, *Nat. Phys.* **16**, 413 (2020).
- [10] M. Schlagmüller, T. C. Liebisch, F. Engel, K. S. Kleinbach, F. Böttcher, U. Hermann, K. M. Westphal, A. Gaj, R. Löw, S. Hofferberth, T. Pfau, J. Pérez-Ríos, and C. H. Greene, *Phys. Rev. X* **6**, 031020 (2016).
- [11] F. Camargo, R. Schmidt, J. D. Whalen, R. Ding, G. Woehl, S. Yoshida, J. Burgdörfer, F. B. Dunning, H. R. Sadeghpour, E. Demler, and T. C. Killian, *Phys. Rev. Lett.* **120**, 083401 (2018).
- [12] M. Tomza, K. Jachymski, R. Gerritsma, A. Negretti, T. Calarco, Z. Idziaszek, and P. S. Julienne, *Rev. Mod. Phys.* **91**, 035001 (2019).
- [13] U. Bissbort, D. Cocks, A. Negretti, Z. Idziaszek, T. Calarco, F. Schmidt-Kaler, W. Hofstetter, and R. Gerritsma, *Phys. Rev. Lett.* **111**, 080501 (2013).
- [14] R. Gerritsma, A. Negretti, H. Doerk, Z. Idziaszek, T. Calarco, and F. Schmidt-Kaler, *Phys. Rev. Lett.* **109**, 080402 (2012).
- [15] J. Joger, A. Negretti, and R. Gerritsma, *Phys. Rev. A* **89**, 063621 (2014).
- [16] H. Doerk, Z. Idziaszek, and T. Calarco, *Phys. Rev. A* **81**, 012708 (2010).
- [17] L. H. Nguyễn, A. Kalev, M. D. Barrett, and B.-G. Englert, *Phys. Rev. A* **85**, 052718 (2012).
- [18] T. Secker, R. Gerritsma, A. W. Glaetzle, and A. Negretti, *Phys. Rev. A* **94**, 013420 (2016).
- [19] R. Côté, V. Kharchenko, and M. D. Lukin, *Phys. Rev. Lett.* **89**, 093001 (2002).
- [20] P. Massignan, C. J. Pethick, and H. Smith, *Phys. Rev. A* **71**, 023606 (2005).
- [21] Y. Sherkunov, B. Muzykantskii, N. d'Ambrumenil, and B. D. Simons, *Phys. Rev. A* **79**, 023604 (2009).
- [22] J. Goold, M. Krych, Z. Idziaszek, T. Fogarty, and T. Busch, *New J. Phys.* **12**, 093041 (2010).
- [23] J. M. Schurer, P. Schmelcher, and A. Negretti, *Phys. Rev. A* **90**, 033601 (2014).
- [24] J. M. Schurer, A. Negretti, and P. Schmelcher, *New J. Phys.* **17**, 083024 (2015).
- [25] Z. Idziaszek, T. Calarco, and P. Zoller, *Phys. Rev. A* **76**, 033409 (2007).
- [26] Z. Idziaszek, A. Simoni, T. Calarco, and P. S. Julienne, *New J. Phys.* **13**, 083005 (2011).
- [27] B. Gao, *Phys. Rev. Lett.* **104**, 213201 (2010).
- [28] B. Gao, *Phys. Rev. A* **83**, 062712 (2011).
- [29] B. Gao, *Phys. Rev. A* **88**, 022701 (2013).
- [30] A. Simoni and J.-M. Launay, *J. Phys. B* **44**, 235201 (2011).
- [31] V. S. Melezhik and A. Negretti, *Phys. Rev. A* **94**, 022704 (2016).
- [32] S. Shadmehri and V. S. Melezhik, *Phys. Rev. A* **99**, 032705 (2019).
- [33] M. Krych, W. Skomorowski, F. Pałowski, R. Moszynski, and Z. Idziaszek, *Phys. Rev. A* **83**, 032723 (2011).
- [34] M. Tomza, C. P. Koch, and R. Moszynski, *Phys. Rev. A* **91**, 042706 (2015).
- [35] M. Tomza, *Phys. Rev. A* **92**, 062701 (2015).
- [36] M. Gacesa and R. Côté, *Phys. Rev. A* **95**, 062704 (2017).
- [37] W. Casteels, J. Tempere, and J. T. Devreese, *J. Low Temp. Phys.* **162**, 266 (2011).
- [38] A. Negretti, R. Gerritsma, Z. Idziaszek, F. Schmidt-Kaler, and T. Calarco, *Phys. Rev. B* **90**, 155426 (2014).
- [39] J. M. Schurer, A. Negretti, and P. Schmelcher, *Phys. Rev. Lett.* **119**, 063001 (2017).
- [40] M. Sroczynska, T. Wasak, K. Jachymski, T. Calarco, and Z. Idziaszek, *Phys. Rev. A* **98**, 012708 (2018).
- [41] W. G. Rellergert, S. T. Sullivan, S. Kotochigova, A. Petrov, K. Chen, S. J. Schowalter, and E. R. Hudson, *Phys. Rev. Lett.* **107**, 243201 (2011).
- [42] J. Deiglmayr, A. Göritz, T. Best, M. Weidemüller, and R. Wester, *Phys. Rev. A* **86**, 043438 (2012).
- [43] F. H. J. Hall and S. Willitsch, *Phys. Rev. Lett.* **109**, 233202 (2012).
- [44] F. H. Hall, M. Aymar, M. Raoult, O. Dulieu, and S. Willitsch, *Mol. Phys.* **111**, 1683 (2013).
- [45] J. Joger, H. Fürst, N. Ewald, T. Feldker, M. Tomza, and R. Gerritsma, *Phys. Rev. A* **96**, 030703(R) (2017).
- [46] M. Krych and Z. Idziaszek, *Phys. Rev. A* **91**, 023430 (2015).
- [47] R. Szmytkowski, *J. Phys. A: Math. Gen.* **28**, 7333 (1995).
- [48] E. Fermi, *Ric. Sci.* **7**, 13 (1936).
- [49] K. Huang, *Statistical Mechanics* (Wiley, New York, 1987).
- [50] K. Jachymski, M. Krych, P. S. Julienne, and Z. Idziaszek, *Phys. Rev. Lett.* **110**, 213202 (2013).

- [51] Z. Idziaszek and T. Calarco, [Phys. Rev. A **71**, 050701\(R\) \(2005\)](#).
- [52] C. Chin, R. Grimm, P. Julienne, and E. Tiesinga, [Rev. Mod. Phys. **82**, 1225 \(2010\)](#).
- [53] E. L. Bolda, E. Tiesinga, and P. S. Julienne, [Phys. Rev. A **66**, 013403 \(2002\)](#).
- [54] D. Blume and C. H. Greene, [Phys. Rev. A **65**, 043613 \(2002\)](#).
- [55] R. Stock, I. H. Deutsch, and E. L. Bolda, [Phys. Rev. Lett. **91**, 183201 \(2003\)](#).
- [56] Z. Idziaszek, T. Calarco, P. S. Julienne, and A. Simoni, [Phys. Rev. A **79**, 010702\(R\) \(2009\)](#).
- [57] J. J. Sakurai, *Modern Quantum Mechanics* (Addison-Wesley, Reading, 1994).
- [58] T. Busch, B. Englert, K. Rzazewski, and M. Wilkens, [Found. Phys. **28**, 549 \(1998\)](#).
- [59] Z. Idziaszek and T. Calarco, [Phys. Rev. A **74**, 022712 \(2006\)](#).
- [60] *Mathematica* (Wolfram Research, Inc., Champaign, 2017), Version 11.1.